Rheologica Acta (2023) 62:239–251
https://doi.org/10.1007/s00397-023-01389-w

ORIGINAL CONTRIBUTION

Two-dimensional glass transition–like behavior of Janus particle–laden interface

Elton L. Correia[1] · H. Henning Winter[2] · Sepideh Razavi[1]

Received: 29 October 2022 / Revised: 21 January 2023 / Accepted: 3 February 2023 / Published online: 22 March 2023

Abstract

Understanding the interactive behavior of Janus particles (JPs) is a growing field of research. The enhancement in binding energy, in comparison to homogenous particles, and the dual characteristic of JPs open up new possibilities for novel applications. In many such applications, interfacial materials become subjected to flows that produce dilational and shear stresses. Therefore, it is important to understand the impact that the Janus character brings to interfaces. In this work, we study the microstructure of two-dimensional (2D) JP monolayers formed at the air–water interface and examine the shear viscoelasticity with an interface rheometer that was adapted for in situ surface pressure control via a Langmuir trough. We extend concepts from bulk rheology to data obtained from interfacial rheology as a tool to understand and predict the monolayer's viscoelastic behavior. Finally, by calculating the time relaxation spectrum from the measured 2D dynamic moduli, we conclude that a phenomenon similar to glass transition is taking place by analogy.

Keywords Janus particles · Particle-laden fluid interfaces · Interfacial rheology · Time-pressure superposition · BSW spectrum

Introduction

The behavior of colloidal particles in vicinity of fluid interfaces has intrigued scientists since the early 1900s (Ramsden 1904; Pickering 1907). By binding to the interface, particles replace the energetically unfavorable contact area between the two fluids with a solid–fluid interface, thus reducing the overall free energy of the system. The large binding energy, relative to the thermal energy, causes particles to irreversibly adsorb at the interface (Park and Lee 2014; Kaz 2011; Zang et al. 2010; Komura et al. 2006; Bresme and Oettel 2007). In a vast range of applications, particles are used to engineer the performance of interfacial systems including pharmaceutics, food stabilization, oil recovery, and personal care products (Mendoza et al. 2014; Binks and Horozov 2006; Aveyard et al. 2003; Crossley et al. 2010; Chen et al. 2018a, b; Qian et al. 2019; Binks 2017; Liu et al. 2018; Kim et al. 2011). In many such applications, interfacial materials become subjected to shear flows and the interface does not remain static; therefore, the response of particle-laden interfaces under applied stresses is of critical importance for the stability of interfacial systems. As such, parameters including particle size, wettability, and concentration have been employed to alter the stability of emulsions and foams (Vishal and Ghosh 2019; Hu et al. 2018; Weston et al. 2015; Zhou et al. 2011; Owoseni et al. 2016; Xue et al. 2016; Arab et al. 2018; Katepalli and Bose 2014; Fan and Striolo 2012; Hunter et al. 2008; Spicer and Gilchrist 2015). Bulk rheological studies have been used to understand the properties of colloidal systems. For example, Katepalli et al. (2017) investigated the rheological behavior of Pickering emulsions stabilized by either spherical or fractal-like particles. It was demonstrated that by tuning the interparticle interactions of fractal-like particles from repulsive to attractive, the emulsion viscosity increased by one order of magnitude, whereas for spherical particles no appreciable difference was found (Katepalli et al. 2017).

The two-dimensional rheology of interfaces has been used to corroborate stability mechanisms impacting the resulting

✉ Sepideh Razavi
srazavi@ou.edu

[1] School of Chemical, Biological, and Materials Engineering, University of Oklahoma, 100 E. Boyd Street, Norman, OK 73019, USA

[2] Department of Chemical Engineering and Department of Polymer Science and Engineering, University of Massachusetts Amherst, Amherst, MA 01003, USA

performance of multi-component systems. Cicuta et al. (2003) showed that the elastic modulus of highly concentrated protein monolayers (β-lactoglobulin) at an air–water interface scales linearly with surface concentration. The authors relate this result to a parallel in 3D, where compressed emulsions at concentrations above the random close packing exhibit a similar behavior (Cicuta et al. 2003). Soft-glassy behavior, reported to occur for asphaltene-populated hexadecane–water surfaces (~2 molecules/nm^2), is shown to be responsible for the prevention of drop coalescence (Samaniuk et al. 2015). Similarly, unique rheological features have also been reported for particle-laden interfaces by altering the interparticle interactions via particle size, wettability, roughness, and shape, and the fluid properties such as pH and electrolytic strength (Manga et al. 2016; Alvarez et al. 2012). For instance, Van Hooghten et al. (2013) reported that rough carbon black particles (33 and 62 nm) present at an octane–water interface formed a monolayer that exhibited an attractive glassy behavior, which aged with time yielding a more elastic interface (Van Hooghten et al. 2013). Maestro et al. (2015) demonstrated that hydrophobic modification of silica nanoparticles (diameter of 30 nm) with surfactants increased their surface coverage and switched the surface behavior from fluid-like to solid-like, with 2D glass properties (Maestro et al. 2015). Shear-thinning behavior has been reported for percolating particle-laden interfaces at surface coverages below jamming (Barman and Christopher 2014). Polystyrene particles (diameter 3.1 ± 0.2 μm) were studied at the air–water interface (3-phase contact angle of $\theta_E = 117°$), where the presence of a monovalent salt in the sub-phase (0.4 M NaCl) screened the repulsive interparticle interactions and allowed for the formation of dense particle aggregates strongly bound to the interface. Shear-thinning behavior at low surface coverage ($\Gamma = 0.6$) was attributed to the breakup of initially densely packed aggregates into smaller disordered clusters upon increasing the shear rate. At higher surface coverages ($\Gamma > 0.7$), some degree of shear induced ordering of particles into hexagonal packing was observed. The existence of a slip plane separating high and low shear rate zones was an indicator that the shear thinning behavior stems from yielding of the particle layer at the interface (Barman and Christopher 2014). Shape anisotropic particles have also been studied at air–water interfaces (Beltramo et al. 2017; Bertsch et al. 2018; Trevenen et al. 2022). Beltramo et al. (2017) demonstrated a significant yield stress in interfacial networks of shape anisotropic particles (polystyrene ellipsoids 2.48-μm long and 0.45-μm wide), much higher than for spherical particles at the same interfacial coverage (Beltramo et al. 2017). This was sufficient to halt bubble dissolution and can be utilized in the design of Pickering foams with excellent stability to reduce bubble Ostwald ripening. A more comprehensive review on the rheology of particle-laden interfaces can be found elsewhere (Derkach et al. 2009; Fuller and Vermant 2012; Jaensson and Vermant 2018; Correia et al. 2021).

With the recent advancements in synthesis and fabrication techniques, colloidal particles can be rendered chemically anisotropic where one face of the particle has one chemistry and the other has another chemistry (Pawar and Kretzschmar 2010; Zhang et al. 2017; Duguet et al. 2016; Walther and Müller 2013; Lattuada and Hatton 2011). Such Janus particles (JPs), named after a two-faced Roman God, are particles that possess dual surface characteristics. This opens up another avenue for tuning the behavior of particles at fluid interfaces. Due to the Janus "motif," these particles can exhibit an enhanced binding energy to the interface compared to a similar sized homogeneous particle (Binks and Fletcher 2001), and their surfaces can be designed to provide added functionalities such as optical, magnetic, and catalytic properties that are anisotropic and directional (Jones et al. 2010; Kim et al. 2013; Shah et al. 2015; Kang and Honciuc 2018; Chen et al. 2018a, b; Nai et al. 2017). The use of JPs in interfacial applications is of particular interest (Kumar et al. 2013; Bradley et al. 2017; Razavi et al. 2015) since they can combine the colloidal-scale properties of particle stabilizers (i.e., large desorption energy from fluid interfaces) (Binks and Fletcher 2001; Binks 2002) with the molecular-scale properties of surfactants (i.e., amphiphilicity and reduction of interfacial tension) (Tu and Lee 2014; Glaser et al. 2006; Park et al. 2013; Fernández-Rodríguez et al. 2016; Fernandez-Rodriguez et al. 2015; Razavi et al. 2020).

The study of JP-laden interfaces is an active area of research to discern the impact of JP attributes such as amphiphilicity and roughness on the microstructure of the resulting network and its interfacial rheology, which can be utilized in engineering the performance of resulting interfacial systems (Kobayashi et al. 2020; Bianchi et al. 2015; DeLaCruz-Araujo et al. 2016; Huang et al. 2019; Kobayashi and Arai 2017; Paiva et al. 2020; Wu et al. 2020). Using a multicomponent Lattice-Boltzmann method, simulations have shown that not only the Janus character and amphiphilicity of the particle affect the rheological properties of the interfacially trapped particle monolayer, but an applied shear flow itself has an impact on the configuration of particles and their assembly. The authors observed the directed assembly of a cluster of randomly oriented spherical JPs into ordered structures at a sheared interface between two immiscible fluids (Rezvantalab et al. 2016). Irrespective of the particle size and for intermediate surface coverages (32–65%), the capillary-induced interactions—resulting from the overlap of the deformed fluid interface under shear flow—yielded particle chain formation normal to the shear direction. Despite the computational studies available on JP-laden interfaces, which indicate their unique rheological properties, experimental studies are still lagging behind. A recent investigation has shown that introducing JPs, at very low concentrations,

to a monolayer populated by homogeneous particles (1:40 Janus-homogeneous ratio) can increase the surface elastic response by one order of magnitude. The change in surface behavior was attributed to the augmented capillary interactions introduced by the JPs' presence in the monolayer (Qiao et al. 2022). A few studies have assessed the response of JP monolayers to dilational stresses (Fernández-Rodríguez et al. 2018; Kadam et al. 2018). For instance, the behavior of poly(methyl methacrylate)/poly-tert-butylmethacrylate (PMMA/PtBMA) Janus particles (diameter of 172 nm) at both air–water and decane–water interfaces was studied in comparison with those obtained from PMMA and PtBMA homogeneous particles. Comparing the surface compression isotherms for the Janus system with their homogeneous counterparts revealed that besides having the highest surface pressure at the entire range of area, Janus particles exhibited a higher static compressional modulus ($\kappa_0{}^s$), indicating the presence of a stronger network (Fernández-Rodríguez et al. 2018). While the shear rheology of particle rafts composed of homogeneous particles has been examined in the literature and the role of particle shape anisotropy on the resulting shear rheology has been highlighted, to the best of our knowledge, experimental studies on the shear rheology of interfaces populated by JPs, which are dominated by capillary interactions, have not yet been reported.

The present study focuses on the behavior of JP monolayers at the air–water interface and their rheological response to applied shear stain and stress. Our goal is to examine the rheological properties of JP monolayers formed at different surface concentrations and demonstrate how existing knowledge on 3D bulk rheology can help to gain understanding of the dynamics of particle-laden interfaces and provide predictive capabilities for other linear viscoelastic material functions. Our data on frequency dependent interfacial rheology demonstrates that the 2D networks of JP-laden air–water interface undergoes a transition that resembles a glass at increased surface pressures.

Methods

Two-dimensional viscoelasticity

In analogy to linear viscoelasticity in three dimensions (Ferry 1980; Tschoegl 2012), two dimensional linear viscoelasticity can be expressed with a stress $\sigma^s(t)$:

$$\sigma^s(t) = \int_{-\infty}^{t} dt' G^s(t-t')\,\dot{\gamma}^s(t') \tag{1}$$

where $\dot{\gamma}^s(t')$ is the rate of deformation in the interfacial layer at past times $-\infty < t' < t$, and

$$G^s(t) = G_0{}^s + \int_0^{\tau_{max}} \frac{d\tau}{\tau} H^s(\tau)\, e^{-t/\tau} \tag{2}$$

is the interfacial relaxation modulus. The interfacial relaxation time spectrum $H^s(\tau)$ quantifies the distribution of relaxation modes that contribute to $G^s(t)$. The largest relaxation time, τ_{max}, belongs to the slowest relaxation mode at long-time stress relaxation.

For practical purposes, the interfacial relaxation modulus may be described by a discrete spectrum with the relaxation strength of g_i corresponding to the relaxation time τ_i as follows:

$$G^s(t) = G_0{}^s + \sum_{i=1}^{N} g_i e^{-t/\tau_i} \tag{3}$$

Small amplitude oscillatory shear (SAOS) results in dynamic moduli:

$$G^{s\prime}(\omega) = G_0{}^s + \int_0^{\tau_{max}} \frac{d\tau}{\tau} H^s(\tau) \frac{\omega^2\tau^2}{1+\omega^2\tau^2} \tag{4}$$

$$G^{s\prime\prime}(\omega) = \int_0^{\tau_{max}} \frac{d\tau}{\tau} H^s(\tau) \frac{\omega\tau}{1+\omega^2\tau^2} \tag{5}$$

These modeling equations will be applied to interfacial rheology experiments in the following manner. The particulate monolayer has no permanent connectivity and rheologically will be treated as a liquid where the equilibrium modulus is zero, $G_0{}^s = 0$. Just like in 3D rheology of viscoelastic liquids, the relaxation time spectrum, $H^s(\tau)$, is the only material property needed for a quantitative description of the two-dimensional linear viscoelasticity of a complex liquid.

Experimental tools and techniques

Interfacial shear rheology setup

A stress-controlled rheometer (DHR2) equipped with the double wall ring (DWR) geometry, mounted inside a Langmuir ribbon trough (L × W = 364 × 75 mm^2), was used to generate the particle-laden interfaces and examine their response to shear at different states of compression (see Fig. 1a). The surface pressure ($\Pi = \sigma^0_{a,w} - \sigma_{a,w}$)—defined as the difference between the air–water surface tension ($\sigma^0_{a,w}$) and the effective surface tension in presence of the particles ($\sigma_{a,w}$)—was measured by a platinum Wilhelmy plate placed parallel to the barriers. The custom design of the jig for the rheometer to accommodate the integrated trough/DWR setup, and the 3D-printed DWR geometry, followed the pioneering work of (Vandebril et al. 2010). The DWR used in this study is a two-dimensional double-Couette fixture

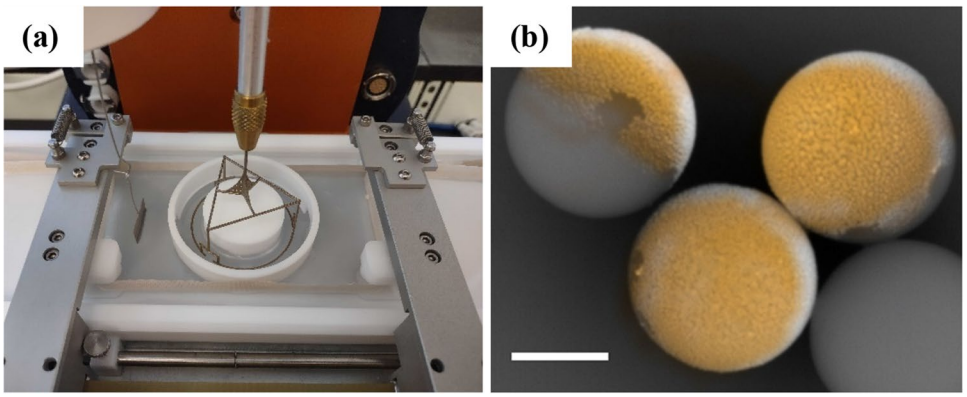

Fig. 1 **a** DWR geometry mounted in a Langmuir ribbon trough used to measure the shear rheology of Janus particle monolayers at the air–water interface. **b** Scanning electron microscope image of Janus particles with gold caps identified by the energy-dispersive X-ray spectroscopy analysis and colored in yellow. Scale bar is 500 nm

(cup) with 39-mm inner diameter, 60-mm outer diameter, and the dimensions of the ring are 47 mm inside diameter and 49 mm outside diameter. The instrument was calibrated in precision mode 4 times to reach a higher sensitivity. The Boussinesq number (Bq) is commonly used to evaluate the balance between surface and subsurface drag (Brenner 2013; Fitzgibbon et al. 2014). To ensure that the subsurface drag is not impacting the generated data, one has to use a geometry that maximizes the contact with the surface minimizing the effect on bulk flow ($Bq > 1$). The DWR geometry used in the current study along with the measured surface viscosities yielded $Bq > 10$ in all cases. Experimental results were analyzed and plotted with the "Interactive Rheology Information System" (IRIS) as outlined in a recent review by (Poh et al. 2022).

Janus particle fabrication and surface modification

Hydrophilic silica particles (1 µm, Fiber Optic Center) are assembled onto a PVC film via a technique called Automated Langmuir–Blodgett, which is a continuous version of the well-known Langmuir–Blodgett method to make a uniform coating on a substrate by transferring the particles from air–water interface to the air–solid interface (Li and Gilchrist 2016). Janus particles were obtained by placing the particle sheets in a physical vapor deposition machine (Lesker Nano36 Evaporator, Kurt J Lesker) and depositing a thin layer of gold (10 nm) mediated by a thin (5 nm) adhesive layer of titanium (see Fig. 1b). To enhance the hydrophobicity of the gold patch, the coated particle monolayers were further modified with octanethiol (Sigma Aldrich) by soaking the slides in 10-mM solution of the thiol in ethanol (Thermo Fisher Scientific) overnight following the procedure used by (Razavi et al. 2019). Next, the particles were washed off the substrate and dispersed in ultrapure deionized (DI) water via sonication, followed by a filtration using a hydrophilic PC membrane filter (10 µm, Isopore™) to remove large aggregates and gold flakes, and finally centrifuged at 3000 rpm for 5 min (Legend X1R, Thermo Scientific). After removing the supernatant, the particles were set to dry under vacuum overnight. DI water (18.2 MΩ.cm) used throughout the study was generated via a Milli-Q® IQ 7000 Ultrapure Lab Water System (Millipore Sigma).

The JP degree of amphiphilicity ($\Delta\theta$) is linked to the difference in the wettability of the polar face (i.e., silica surface, θ_p) and the apolar face (i.e., gold patch, θ_a) as follows $\Delta\theta = \left(\theta_a - \theta_p\right)/2$. To quantify the wettability of each face and assess the JP amphiphilicity, measurements of the 3-phase contact angle were carried out using water droplets deposited on base-cleaned glass substrates and glass substrates that had gone through the same gold deposition and surface modification steps as the particles. Next, the drop shape profile was fitted and analyzed using a tensiometer (Biolin Scientific). The water contact angle on untreated glass slides and gold-coated slide were measured to be $\theta_p = 27 \pm 4°$ and $\theta_a = 76 \pm 6°$, respectively. Upon treatment of the gold-coated slides with octanethiol, the water contact angle increased to $102 \pm 3°$. Therefore, using the values of $\theta_p = 27 \pm 4°$ and $\theta_a = 102 \pm 3°$, the amphiphilicity is estimated to be $\Delta\theta = 38 \pm 5°$ for the Janus particles of this study.

Monolayer preparation

To prepare the particle dispersions, JPs were suspended in a 30/70 wt% water/isopropyl alcohol (Thermo Fisher Scientific) mixture at a concentration of 3.75 g/mL. Initially, the trough area in the open-state was set at 150 cm^2 in all experiments. To ensure the absence of impurities at the air–water interface, the trough was closed to 60 cm^2 and the change in the surface pressure was monitored. If the surface pressure remained negligible ($\Pi < 0.3$ mN/m), deposition of the particles at the interface was carried out as follows. Two hundred microliters of the suspension was deposited at the air–water interface in a dropwise fashion using a 50-µL syringe (Hamilton) and the particles spread at the interface via the action of Marangoni flows. A 30-min wait period was

added to allow for the solvent evaporation before proceeding with the measurements.

Interfacial rheology measurements

After preparing the JP monolayer at the air–water interface on the trough in the open-state (i.e., total surface area of 150 cm^2), the double wall ring (DWR) was slowly lowered to contact the interface via capillary action. The axial load on the ring was carefully monitored while lowering it towards the interface; a sudden increase in the measured force indicated the onset of contact between DWR and interface. Once the initial contact was made, the ring (1-mm thick) was lowered for an additional 500 µm so that the DWR was centered at the interface. The integrated trough/DWR setup enabled us to achieve specific surface pressure values and carry out rheological measurements on particle networks at different surface coverages. The monolayer was compressed at a rate of 25 cm^2/min until reaching a desired surface pressure. The particles were then allowed to relax and reorganize until the surface pressure stabilized (~ 10 min) prior to carrying out the rheological experiments. Strain amplitude sweep and small amplitude oscillatory shear (SAOS) measurements were carried out using this integrated setup to characterize the JP monolayer. The operating windows for the oscillatory measurements that lead to valid reproducible results are calculated following the work of Ewoldt and coworkers (Renggli et al. 2020). These ranges are color coded in the reported figures. In brief, the data falling in the green range represents an acceptable data set, the data falling in the yellow region represents probably acceptable data, and the rest, falling in the orange region, needs to be handled with care.

Microstructure characterization

In order to link the monolayer microstructure, corresponding to different surface pressures, with the resulting interfacial rheology of such network, analogue experiments were carried out via a custom-built trough/microscope setup. A NIMA Langmuir trough (Biolin Scientific) equipped with an imaging window machined in the center was mounted on top of an inverted microscope (IX73 Olympus), the interface was prepared following the exact steps provided earlier, and the imaging of the particle-laden interface was carried out using a 20 × objective (6.6–7.8 WD, 0.45 NA). It is important to note that shear stresses can be generated during monolayer compressions on a Langmuir trough. A shear-stress-free "Quadrutrough" has been recently developed to overcome this issue (Tein et al. 2022).

To evaluate the orientation of the Janus particles residing the air–water interface, deposition of interfacially trapped particles on a silicon wafer was carried out following the work of Razavi et al. (2019). Briefly, a silicon wafer was placed at the bottom of the trough at the beginning of the experiment. After the deposition of particles at the interface and reaching a surface pressure of 5 mN/m via compression, the JP network was transferred from the air–water interface to the silicon wafer substrate by gently aspirating the subphase from the side of the trough, outside the barriers, until the particle monolayer came in contact with the substrate. The deposited monolayer was then imaged via the environmental scanning electron microscope (Thermo Quattro S field-emission SEM). The distribution of the particle orientation was obtained by analyzing ~ 50,000 particles using the HEXI software via brightness thresholding of the particles (Domonkos et al. 2022). To examine whether the use of a spreading solvent in the deposition of particles at the interface, and the associated Marangoni flows, result in ordered crystalline domains, we applied the procedure provided by Juarez et al. (Juárez and Bevan 2012) to the captured SEM images to determine the ensemble average of the order parameter C_6. In short, C_6 represents the number of hexagonal close packed neighbors around each particle. By averaging over all particles, we estimate $<C_6>$, which equals 0 for disordered fluid configurations and 6 for an infinite plane of hexagonal close packed particles. Further details on the calculation of $<C_6>$ are provided in the "Supplementary information".

Experimental results

Surface pressure and microstructure of Janus particles at the air–water interface

The surface pressure isotherm and the accompanying microstructure formed by the Janus particles at various surface pressures are provided in Fig. 2a. As the surface area available for the particles was reduced by closing the barriers, from 150 to 60 cm^2, the surface pressure increased. The microstructure present at lower surface pressures (1 mN/m and 5 mN/m) illustrates large particle clusters with an area spanning open network. Additional pictures of the microstructure at 1 mN/m are provided in the "Supplementary information" Figure S1. The formation of area-spanning dendritic structures by JPs at a fluid interface has been reported by Park et al. (2011) and is attributed to the presence of capillary interactions between Janus particles. Compressing the monolayer further to surface pressure of 10 mN/m and above resulted in the disappearance of the open spaces and yielded a dense surface monolayer that is highly populated by the particles. The surface pressure isotherms obtained from these experiments were in good agreement with measurements carried out on the ribbon trough. The analysis of JPs' orientation distribution with regard to the plane of the interface, performed on the SEM images,

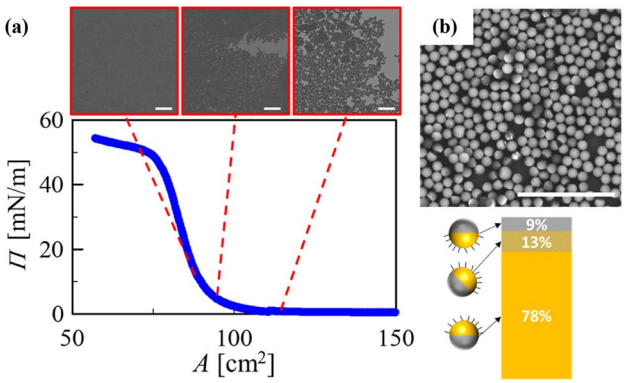

Fig. 2 **a** Surface pressure isotherm for the Janus particle monolayer at the air–water interface; examples of the microstructure formed at different surface pressures and captured by an inverted optical microscope are provided along the isotherm; from right to left the micrographs belong to the surface pressures in increasing order as follows: 1 mN/m, 5 mN/m, and 10 mN/m, respectively. Scale bar is 11 µm. **b** Illustrative SEM picture of Janus particle monolayer at 5 mN/m along with the distribution of the Janus cap orientation with regard to the plane of the interface (i.e., cap up, sideways, and cap down). Scale bar is 10 µm

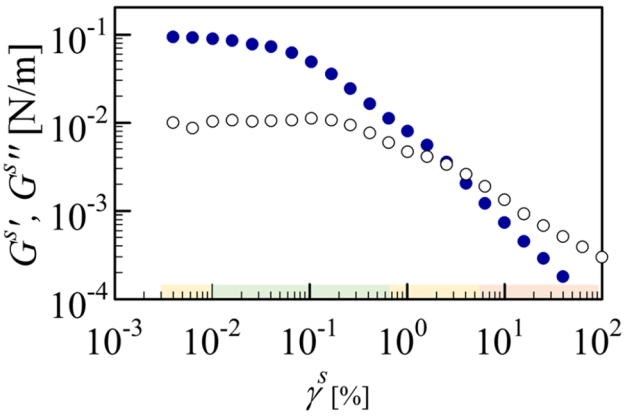

Fig. 3 Dynamic moduli of the JP monolayer at $\Pi = 30$ mN/m, measured at $\omega = 1$ rad/s, with increasing shear strain amplitude γ^s. Colored bars on the horizontal axis depict the operating windows as follows: measured stress/inertia stress is (orange) < 5, (yellow) > 5, and (green) > 10

examples of which are provided in Fig. 2b and Figure S2, shows that 78% of the particles resided at the interface with their gold cap orienting upwards (i.e., the Janus boundary was aligned with the air–water interface). It should be noted that the ensemble averaged value of C_6, obtained over all particles in the monolayer captured within the SEM images, is calculated to be $\sim 2.0 \pm 0.1$, indicating an amorphous structure.

Surface shear rheology of Janus particles at the air–water interface

To identify the linear viscoelastic regime (LVE) for 2D interfacial networks, images of which are provided in Fig. 2, strain amplitude sweeps were performed at 1 rad/s, and in the oscillation shear strain range of 0.001–100%, results of which are provided in Fig. 3. It was found that the connectivity of the JP surface layer is strong enough to support shearing up to a shear strain amplitude of about 0.04%. With the knowledge obtained on the LVE region, the JP monolayer was subjected to a shear frequency sweep and its dynamic response was calculated from the instrument torque. The measured dynamic moduli are shown in Fig. 4 at various surface pressures, which are related to the surface packing of JPs. Small-amplitude oscillatory shear (SAOS) experiments provided reliable modulus data, $G^{s\prime}$ and $G^{s\prime\prime}$, by choosing a shear strain amplitude of 0.03%, which is in the LVE regime as determined earlier (see Fig. 3). The dynamic modulus increases in value as the surface pressure is increased as displayed in Fig. 4.

With the exception of the lowest surface pressure (5 mN/m), which showed particle-void domains within the microstructure (cf. Figure 1), all $G^{s\prime}$ and $G^{s\prime\prime}$ data assume the same shape, for all surface pressures studied, and can be merged into a single set of master curves via a time-pressure superposition (t Π s). The t Π s process follows the classical pattern of 3D time–temperature superposition (Ferry 1980). Data at surface pressure of $\Pi = 30$ mN/m were chosen as reference state for generating the master curves. This required the time shift (horizontal shift factor, a_Π) and the modulus shift (vertical shift factor, b_Π) values of which are provided in Fig. 5. The resulting master curves belonging to the various surface pressures are illustrated in Fig. 6a and expressed as complex viscosity in Fig. 6b. Both shift factors are about equally involved. In this way, the time-pressure superposition (t Π s) of JP monolayer dynamics varies from traditional time–temperature shifting where the vertical shift factor for $G^{s\prime}$ and $G^{s\prime\prime}$ is close to unity for many viscoelastic materials (3D).

The same data are presented in three different ways, always in conjunction with the respective spectrum predictions (Eq. 6). The loss tangent, displayed in Fig. 6c, has the typical format as expected for a liquid. The choice of surface pressure $\Pi = 30$ mN/m as reference state is purely arbitrary. The data can now be shifted to other surface pressures, even to Π values in between, where no experiment has been executed. This free use of the data is possible because of the known t Π s shift functions, values of which are provided in Fig. 5.

The validity of the $G^{s\prime}$, $G^{s\prime\prime}$ data was confirmed using the Kramers–Kronig check (Winter 1997), which involves the calculation of the relaxation time spectrum. At first, the data of Fig. 6 were modeled with the parsimonious model

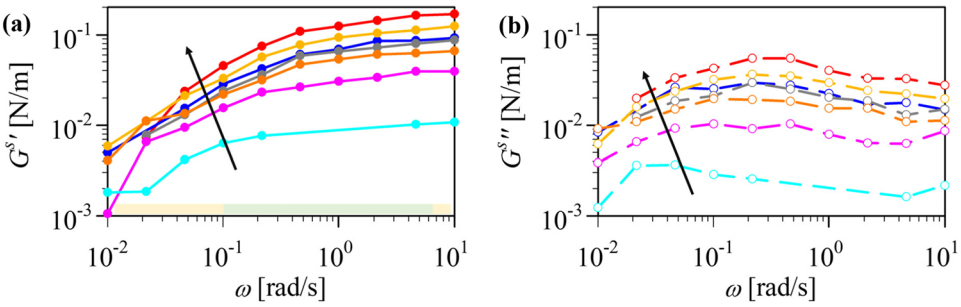

Fig. 4 Dynamic moduli at increasing surface pressure (shown by the arrow) of Π = 5, 10, 15, 20, 30, 40, and 50 mN/m; **a** storage modulus, **b** loss modulus. Colored bars on horizontal axis depict the operating windows as follows: measured stress/inertia stress is (orange) < 5, (yellow) > 5, and (green) > 10

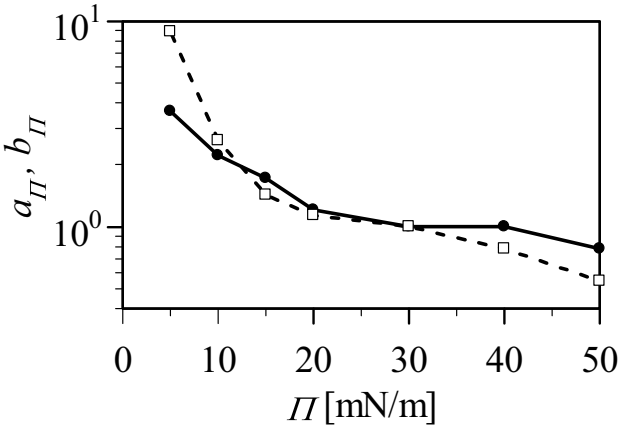

Fig. 5 Horizontal shift factors a_Π (closed symbol) and vertical shift factor b_Π (open symbol). The reference state is Π = 30 mN/m

of Baumgärtel and Winter (1989, 1992), which seeks a discrete relaxation time spectrum (Eq. 3), with the least number of discrete modes for optimal fit (avoiding over-fitting and converts this spectrum into an approximate continuous form. The pattern of the parsimonious spectrum for the JP monolayer suggests a power law format. Inserted into Eqs. 4 and 5, the continuous relaxation time spectrum of the parsimonious model (Baumgärtel and Winter 1989, 1992) was able to fit the experimental $G^{s'}$ and $G^{s''}$ of Figs. 3 and 6a. The shape of the parsimonious relaxation time spectrum (Fig. 7), having a dominant positive slope and a fairly abrupt cutoff, indicates the possibility of a power-law spectrum very much like the BSW spectrum of a colloid near its glass transition (Siebenbürger et al. 2009; Winter 2013). This is expressed as a linear superposition of two power laws. The long-time relaxation behavior (α-mode) belongs to large scale rearrangements in the surface layer, while localized particle rearrangements and their short time characteristics give rise to the faster β-mode:

$$H^s(\tau) = H_\alpha{}^s \left(\frac{\tau}{\tau_{max}}\right)^{n_\alpha} + H_\beta{}^s \left(\frac{\tau}{\tau_\beta}\right)^{-n_\beta} \tag{6}$$

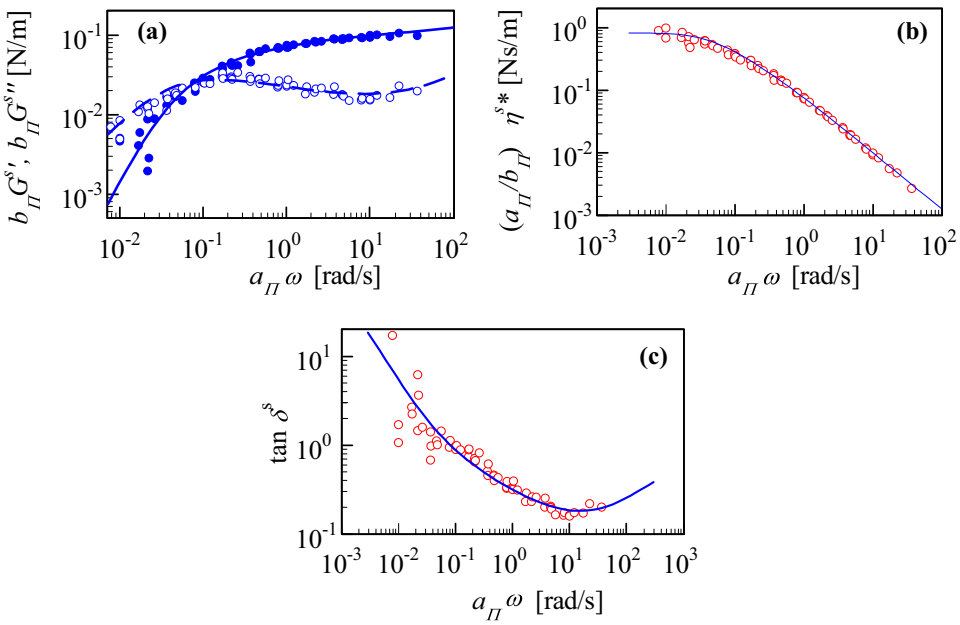

Fig. 6 **a** Dynamic modulus data merged onto Π = 30 mN/m; $b_\Pi G^{s'}(\omega)$ closed symbols, $b_\Pi G^{s''}(\omega)$ open symbols. **b** Complex shear viscosity from master curve at Π = 30 mN/m. **c** tan δ^s for master curve with experimental data as red open circles. The lines belong to the power law relaxation time spectrum (Eq. 6), as discussed in the text, with parameters listed with Fig. 7

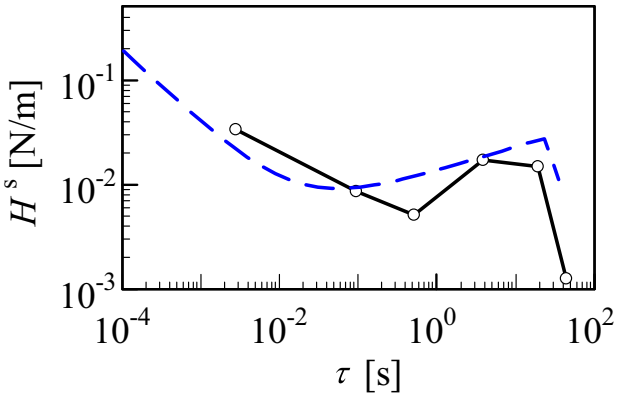

Fig. 7 Continuous relaxation time spectrum $H^s(\tau)$ as determined by parsimonious method (Baumgärtel and Winter 1989, 1992), shown with discrete points, and approximated as continuous function (Eq. 6), shown in dashed line. $\Pi = 30$ mN/m data were approximated with $H_\alpha{}^s = 0.03$ N/m; $\tau_\alpha = 34.7$ s; $n_\alpha = 0.2$; $\tau_\beta = 1.35 \times 10^{-3}$ s; $n_\beta = 0.7$, using a simplified $H_\beta{}^s = H_\alpha{}^s$

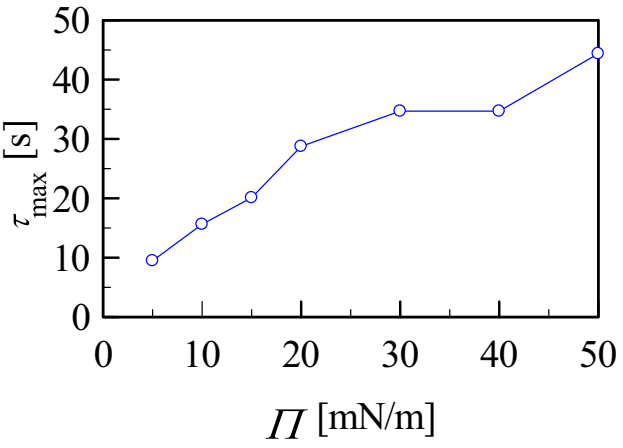

Fig. 8 Dependency of the maximum relaxation time on the surface pressure of the JP monolayer

valid for $\tau \leq \tau_{max}$. Beyond that upper time limit, $\tau_\alpha = \tau_{max}$, the spectrum does not exist, $H^s(\tau) = 0$, for $\tau > \tau_{max}$. τ_β denotes the minimum in the spectrum where the two powerlaws meet. This spectrum was found to closely reproduce the experimental data as shown in Fig. 6 for the $\Pi = 30$ mN/m interface. An overlay of the parsimonious spectrum and the BSW spectrum compares the two in Fig. 7.

The pair of master curves of dynamic moduli for all surface pressures (see Fig. 6a), shifted to 30 mN/m, includes the crossover between $G^{s\prime}$ and $G^{s\prime\prime}$, which characterizes the frequency at which the surface behavior is switched from viscous-dominant to elastic-dominant, all while remaining in the liquid state. It has become common practice to define a nominal longest relaxation time based on the frequency of the $G^{s\prime} = G^{s\prime\prime}$ crossover.

$$\tau_{G^{s\prime}=G^{s\prime\prime}} = \frac{2\pi}{\omega_{G^{s\prime}=G^{s\prime\prime}}} \tag{7}$$

For the JP monolayer of this study, the longest relaxation time is close to $\tau_{G^{s\prime}=G^{s\prime\prime}}$ only slightly smaller:

$$\frac{\tau_{max}}{\tau_{G^{s\prime}=G^{s\prime\prime}}} = 0.42 \tag{8}$$

The value of this ratio depends on material specifics but is the same for all compositions of this study satisfying t Π s. That includes the Janus dynamics (see Fig. 6). The BSW model (Eq. 6 with data of Fig. 7) provides the values of $\tau_{G^{s\prime}=G^{s\prime\prime}}$ and of τ_{max} as appropriate for the experimental data. The values of τ_{max} obtained for different surface pressures are provided in Fig. 8. The relation between τ_{max} and Π was generated by taking the τ_{max} value at the reference state, $\tau_{max} = 34$ s at $\Pi = 30$ mN/m, and shifting it in the same way as $G^{s\prime}$ and $G^{s\prime\prime}$ were shifted to generate the $\Pi = 30$ mN/m master curve.

Linear viscoelastic properties of Janus particle-laden interfaces

The known relaxation time spectrum can now provide predictive capabilities to be used to evaluate linear viscoelastic material functions such as the relaxation modulus $G^s(t)$, as defined in Eq. 2, and the creep compliance $J^s(t)$. For this, we use the relaxation time spectrum as calculated with the parsimonious model in comparison to BSW. The time-dependent relaxation modulus and creep compliance (Fig. 9) are very similar for the two models of the relaxation time spectrum presented in Fig. 7.

The SAOS experiments did not allow us to increase the frequency to a level where more of the β-dynamics would govern as the geometry inertia takes place. It is outside our SAOS range, while barely showing the onset of β-dynamics as the upper end of the ω-window. Dedicated high-frequency methods would be needed to learn more about the β-dynamics, which is outside the focus of the current study. In consideration of this limitation, little information is available here about the β-modes since $G^{s\prime}$ and $G^{s\prime\prime}$ data were taken in a frequency range were the α-modes dominate. Without accounting for the β-modes, the zero-shear surface viscosity reduces to:

$$\eta_0{}^s = \frac{H_\alpha{}^s \tau_{max}}{1 + n_\alpha} \tag{9}$$

The corresponding zero-shear compliance calculates as:

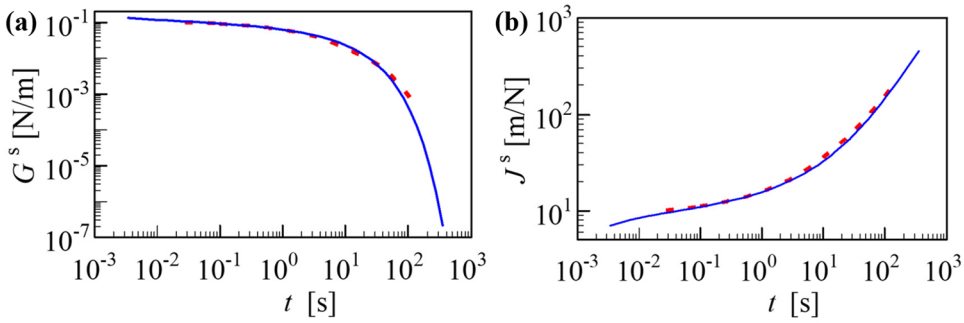

Fig. 9 The known relaxation time spectra allow predictions of other linear viscoelastic functions for $\Pi = 30$ mN/m dynamics: **a** relaxation modulus, **b** creep compliance; dotted lines for parsimonious spectrum and continuous lines for BSW power law relaxation time spectrum (Eq. 6) and parameter values as listed in Fig. 7

$$J_0^s = \frac{n_\alpha}{H_\alpha^s}\left(1 + \frac{1}{2n + n^2}\right) \tag{10}$$

These are a few examples. The choice of $\Pi = 30$ mN/m is arbitrary. With the given spectrum, we can equally predict properties at the other surface pressures, or in between, as long as they satisfy the t Π s. Material functions as shown here are useful for advancing application examples which were provided in the "Introduction."

Discussion

The relaxation time spectrum of interfacial layers formed by Janus particles (Eq. 6) is new for 2D viscoelasticity, but it is exactly the same as was found earlier in 3D viscoelasticity. There, it defines the dynamics of the colloidal glass transition in three dimensions (Siebenbürger et al. 2009). Macroscopically, the colloidal dynamics of the 3D glass transition is re-occurring in the two-dimensional viscoelasticity of the Janus particle monolayer. From these findings, and due to the similarity to the 3D phenomenon, we infer that the interfacial assembly of Janus particles undergoes a transition analogous to a 2D glass.

As previously discussed by Winter (2013), the relaxation time spectrum for glass transition and gelation phenomena of bulk materials broadens and assumes a power law format. However, the power law exponent is positive for glass transitions and negative for gelation near the transition. This distinguishing difference originates from the fact that gel rheology is dominated by fast modes of relaxation, whereas glass transitions are dominated by slow modes of larger patches (Winter 2013). Therefore, the fact that H^s obtained for the Janus particle monolayer at 30 mN/m has a positive slope, corroborates the idea that a transition analogous to a glass is taking place.

The re-appearance of the BSW spectrum is really striking. There seems a common rheological pattern in viscoelastic liquids when caging dominates their dynamics. The BSW spectrum has occurred in polymeric liquids with long linear flexible molecules of uniform length (Baumgärtel et al. 1990). There, polymer molecules are envisioned to be caged by neighboring molecules in a tube-like constraint (Doi and Edwards 1986). In this study, 2D dynamics of the Janus particles at the interface involves constraining by neighboring particles, which can be envisioned as two-dimensional caging. To go even further, the glass transition of colloids can also be envisioned as a caging process, which will occur in three dimensions and also is governed by BSW dynamics. Caging is the common feature that might connect all three. However, as the capillary interactions governing the monolayer of JPs of this work are dependent on the orientation of the Janus patches as the particles approach each other, and because densification of the particles at higher surface pressures constrains their reorientation at the interface, both attractive and repulsive capillary interactions may be present between the particles throughout the interfacial monolayer. Therefore, the 2D cages present in our experiments are more complex and harder to define as further elaborated below.

Janus particles at fluid interfaces tend to present microstructures dominated by capillary interactions (Park et al. 2011; Guzmán et al. 2022). These capillary interactions are usually of high-order multipoles (either quadrupoles or hexapoles) as monopolar interactions are negligible for micron-sized particles ($\sim 10^{-7}\ k_B$T) and dipolar interactions are neglected for homogeneous particles (Danov et al. 2005). However, as shown in the SEM pictures of the microstructure and their analysis (cf. Figure 1b), not all the particles have their Janus boundary aligned with the surface. The presence of tilted particles introduces dipolar capillary interactions (Rezvantalab and Shojaei-Zadeh 2013), which in addition to the higher order capillary interactions dictate the overall microstructure. Moreover, while the capillary interactions between particles separated at large distances are attractive because the particles are able to reorient themselves with the generated torque, at smaller distances, and with the many-body interactions present in a dense monolayer, particles might not be able to reorient; thus, the lateral capillary interactions in the near field can even be repulsive. This is also evidenced in Fig. 8, where by increasing the surface pressure the maximum relaxation time increases, indicating larger structures that take longer to relax. Therefore, a

complex network arises from these capillary interactions, which yields the interfacial rheological behavior reported in this work. The role of the particle orientation distribution on the resulting microstructure and its consequence for interfacial rheology of the JP monolayer are under investigation for particles of different amphiphilicity and will be reported in a follow up publication.

As shown in Fig. 2, the particle surface coverage is increased by compressing the surface area, as expected. From the Langmuir trough measurements, it is possible to note that most of the surface is occupied by particles at 10 mN/m, indicating that the surface coverage does not change considerably upon further compression. However, from the rheological measurements, there is an increase in $G^{s'}$ as the surface pressure is increased, which has been related to an increase in surface coverage (Beltramo et al. 2017). We attribute this difference in behavior to the high interfacial shear viscosity of the monolayer, which can lead to a heterogeneous pressure distribution along the interface, specifically through the side openings of the geometry cup. Therefore, differences could exist between the surface pressure inside the cup and the value obtained from the Wilhelmy plate residing outside the cup.

The shear response of monolayers at interfaces is frequently weaker when compared to that of bulk materials. For that reason, measurements are usually taken close to the lower torque limits of rheometers. In addition, the subphase drag contribution might introduce noise into the system if one is operating at low values of *Bq* number (Renggli et al. 2020). To account for the subphase contribution, flow field calculations were developed by Vandebril et al. to correct the apparent shear rate taking into account the coupling of bulk and interface (Vandebril et al. 2010). In short, the algorithm consists of solving the velocity profile at the interface and in the subphase numerically, and estimating the drag contribution from the subsurface, which allows for its removal from the raw data. As stated in Vandebril et al., $Bq >> 100$ is desired when conducting interfacial rheology measurements to ensure negligible contributions from subphase drag (Vandebril et al. 2010). Therefore, we applied the subphase correction to decouple the interfacial contribution from the bulk generated drag and examine the significance of the bulk contribution in the generated data. The comparison between the raw data and the sub-phase corrected data is provided in Fig. 10, which illustrates that the master curve obtained from both data sets are in good agreement.

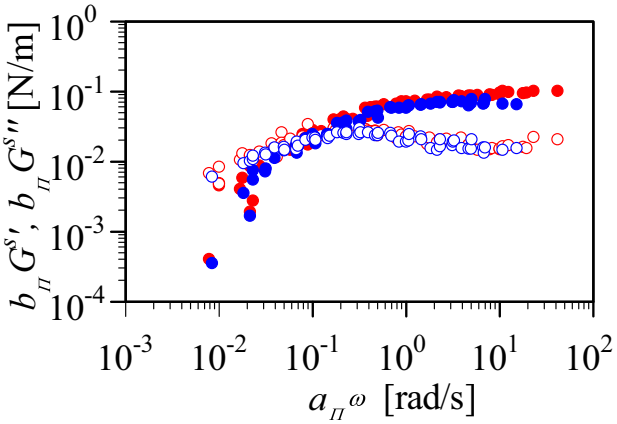

Fig. 10 Comparison of the master curves generated by the raw data and the subphase-corrected data obtained using the algorithm by Vandebril et al. Red is the raw data and blue the corrected data

Conclusions

In this work, we measured the surface shear rheology of a Janus particle monolayer at the air–water interface as a function of the surface pressure. The interfacially trapped particle network was analyzed from different aspects, including the relation between the microstructure and surface pressure, and the orientation distribution of the Janus boundary at the interface. Our results show that the majority of the particles (78%) are residing the interface with their Janus cap aligned with the interface, which results in a compact network formed at the air–water interface via the effect of capillary interactions. Additionally, we demonstrated how classical rheology analysis can be applied to the generated small amplitude oscillatory shear data obtained in 2D such as the Janus particle monolayers of this study. The data obtained at various surface pressures were collapsed into a master curve via a time-pressure superposition (t Π s). By analyzing the time relaxation spectrum, we have found that a transition that resembles that of a glass transition is occurring in the interfacial network of Janus particles. The time-relaxation spectrum further provides us with predictive capabilities and allows us to describe additional linear viscoelastic material functions for two-dimensional materials that can be useful in the rational design of formulations tailored to different applications.

Supplementary Information The online version contains supplementary material available at https://doi.org/10.1007/s00397-023-01389-w.

Acknowledgements SR and EC would like to thank Prof. James Gilchrist from Lehigh University for providing the PVC sheets coated with the silica particles, which were then used in the fabrication of Janus particles in our laboratory. EC acknowledges the support of the National Association for Surface Finishing (NASF) for the graduate scholarship. SR and EC acknowledge the support from the American Chemical Society, Petroleum Research Fund, through grant PRF # 61617-DNI9 and the National Science Foundation under award # CBET-1934513. HHW acknowledges support for this work by the U.S. Department of Energy, Office of Energy Efficiency and Renewable Energy, Bioenergy Technologies Office under award # DE-EE0009285. Financial support was provided by the University of Oklahoma Libraries' Open Access fund.

Declarations

Conflict of Interest The authors declare no competing interests.

References

Alvarez NJ, Anna SL, Saigal T, Tilton RD, Walker LM (2012) Interfacial dynamics and rheology of polymer-grafted nanoparticles at air–water and xylene–water interfaces. Langmuir 28:8052–8063

Arab D, Kantzas A, Bryant SL (2018) Nanoparticle stabilized oil in water emulsions: a critical review. J Petrol Sci Eng 163:217–242

Aveyard R, Binks BP, Clint JH (2003) Emulsions stabilised solely by colloidal particles. Adv Coll Interface Sci 100–102:503–546

Barman S, Christopher GF (2014) Simultaneous interfacial rheology and microstructure measurement of densely aggregated particle laden interfaces using a modified double wall ring interfacial rheometer. Langmuir 30:9752–9760

Baumgärtel M, Winter HH (1989) Determination of discrete relaxation and retardation time spectra from dynamic mechanical data. Rheol Acta 28:511–519

Baumgärtel M, Winter HH (1992) Interrelation between continuous and discrete relaxation time spectra. J Non-Newtonian Fluid Mech 44:15–36

Baumgärtel M, Schausberger A, Winter HH (1990) The relaxation of polymers with linear flexible chains of uniform length. Rheol Acta 29:400–408

Beltramo PJ, Gupta M, Alicke A, Liascukiene I, Gunes DZ, Baroud CN, Vermant J (2017) Arresting dissolution by interfacial rheology design. Proc Natl Acad Sci 114:10373–10378

Bertsch P, Diener M, Adamcik J, Scheuble N, Geue T, Mezzenga R, Fischer P (2018) 'Adsorption and interfacial layer structure of unmodified nanocrystalline cellulose at air/water interfaces'. Langmuir 34:15195–202

Bianchi E, Panagiotopoulos AZ, Nikoubashman A (2015) Self-assembly of Janus particles under shear. Soft Matter 11:3767–3771

Binks BP (2002) Particles as surfactants—similarities and differences. Curr Opin Colloid Interface Sci 7:21–41

Binks BP (2017) Colloidal particles at a range of fluid–fluid interfaces. Langmuir 33:6947–6963

Binks BP, Fletcher PDI (2001) particles adsorbed at the oil−water interface: a theoretical comparison between spheres of uniform wettability and "janus" particles. Langmuir 17:4708–4710

Binks BP, Horozov TS (2006) Colloidal particles at liquid interfaces. Cambridge University Press

Bradley LC, Chen W-H, Stebe KJ, Lee D (2017) Janus and patchy colloids at fluid interfaces. Curr Opin Colloid Interface Sci 30:25–33

Brenner H (2013) Interfacial transport processes and rheology (Elsevier), p 134

Bresme F, Oettel M (2007) Nanoparticles at fluid interfaces. J Phys: Condens Matter 19:413101

Chen CL, Wang SS, Kadhum MJ, Harwell JH, Shiau BJ (2018a) Using carbonaceous nanoparticles as surfactant carrier in enhanced oil recovery: a laboratory study. Fuel 222:561–568

Chen D, Zhang G, Torquato S (2018b) Inverse design of colloidal crystals via optimized patchy interactions. J Phys Chem B 122:8462–8468

Cicuta P, Stancik EJ, Fuller GG (2003) Shearing or compressing a soft glass in 2D: time-concentration superposition. Phys Rev Lett 90:236101

Correia EL, Brown N, Razavi S (2021) Janus particles at fluid interfaces: stability and interfacial rheology. Nanomaterials 11:374

Crossley S, Faria J, Shen M, Resasco DE (2010) Solid Nanoparticles that Catalyze Biofuel Upgrade Reactions at the Water/Oil Interface. Science 327:68–72

Danov KD, Kralchevsky PA, Naydenov BN, Brenn G (2005) Interactions between particles with an undulated contact line at a fluid interface: capillary multipoles of arbitrary order. J Colloid Interface Sci 287:121–134

DeLaCruz-Araujo RA, Beltran-Villegas DJ, Larson RG, Córdova-Figueroa UM (2016) Rich Janus colloid phase behavior under steady shear. Soft Matter 12:4071–4081

Derkach SR, Krägel J, Miller R (2009) Methods of measuring rheological properties of interfacial layers (experimental methods of 2D rheology). Colloid J 71:1–17

Doi M, Edwards SF (1986) Theory of polymer dynamics. Clarendon Press, Oxford Press

Domonkos M, Jackivová R, Pathó A (2022) Image analysis algorithm for the verification of hexagonal symmetry in spherical nanostructures. Microelectron Eng 251:111635

Duguet É, Hubert C, Chomette C, Perro A, Ravaine S (2016) Patchy colloidal particles for programmed self-assembly. C R Chim 19:173–182

Fan H, Striolo A (2012) Mechanistic study of droplets coalescence in Pickering emulsions. Soft Matter 8:9533–9538

Fernandez-Rodriguez MA, Ramos J, Isa L, Rodriguez-Valverde MA, Cabrerizo-Vilchez MA, Hidalgo-Alvarez R (2015) Interfacial activity and contact angle of homogeneous, functionalized, and Janus nanoparticles at the water/decane interface. Langmuir 31:8818–8823

Fernández-Rodríguez MA, Percebom AM, Giner-Casares JJ, Rodríguez-Valverde MA, Cabrerizo-Vílchez MA, Liz-Marzán LM, Hidalgo-Álvarez R (2016) Interfacial activity of gold nanoparticles coated with a polymeric patchy shell and the role of spreading agents. ACS Omega 1:311–317

Fernández-Rodríguez MÁ, Rahmani S, Yu CKJ, Rodríguez-Valverde MÁ, Cabrerizo-Vílchez MÁ, Michel CA, Lahann J, Hidalgo-Álvarez R (2018) Synthesis and interfacial activity of PMMA/PtBMA Janus and homogeneous nanoparticles at water/oil interfaces. Colloids Surf, A 536:259–265

Ferry JD (1980) Viscoelastic properties of polymers. John Wiley & Sons

Fitzgibbon S, Shaqfeh ESG, Fuller GG, Walker TW (2014) Scaling analysis and mathematical theory of the interfacial stress rheometer. J Rheol 58:999–1038

Fuller GG, Vermant J (2012) Complex fluid-fluid interfaces: rheology and structure. Annu Rev Chem Biomol Eng 3:519–543

Glaser N, Adams DJ, Böker A, Krausch G (2006) Janus particles at liquid−liquid interfaces. Langmuir 22:5227–5229

Guzmán E, Ortega F, Rubio RG (2022) Forces controlling the assembly of particles at fluid interfaces. Langmuir 38(44):13313–13321

Hooghten V, Rob LI, Boeckx V, Sharma R, Vermant J (2013) Rough nanoparticles at the oil–water interfaces: Their structure, rheology and applications. Soft Matter 9:10791–10798

Hu N, Li Y, Zhaoliang Wu, Ke Lu, Huang Di, Liu W (2018) Foams stabilization by silica nanoparticle with cationic and anionic surfactants in column flotation: Effects of particle size. J Taiwan Inst Chem Eng 88:62–69

Huang Z, Zhu G, Chen P, Hou C, Yan L-T (2019) Plastic crystal-to-crystal transition of Janus particles under shear. Phys Rev Lett 122:198002

Hunter T, Pugh R, Franks G, Jameson G (2008) The role of particles in stabilising foams and emulsions. Adv Coll Interface Sci 137:57–81

Jaensson N, Vermant J (2018) Tensiometry and rheology of complex interfaces. Curr Opin Colloid Interface Sci 37:136–150

Jones MR, Macfarlane RJ, Lee B, Zhang J, Young KL, Senesi AJ, Mirkin CA (2010) DNA-nanoparticle superlattices formed from anisotropic building blocks. Nat Mater 9:913–917

Juárez JJ, Bevan MA (2012) Feedback controlled colloidal self-assembly. Adv Funct Mater 22:3833–39

Kadam R, Zilli M, Maas M, Rezwan K (2018) Nanoscale Janus Particles with Dual Protein Functionalization. Part Part Syst Charact 35:1700332

Kang C, Honciuc A (2018) Self-assembly of Janus nanoparticles into transformable suprastructures. The Journal of Physical Chemistry Letters 9:1415–1421

Katepalli H, Bose A (2014) Response of Surfactant Stabilized Oil-in-Water Emulsions to the Addition of Particles in an Aqueous Suspension. Langmuir 30:12736–12742

Katepalli H, John VT, Tripathi A, Bose A (2017) Microstructure and rheology of particle stabilized emulsions: Effects of particle shape and inter-particle interactions. J Colloid Interface Sci 485:11–17

Kaz DM (2011) Colloidal particles and liquid interfaces: A spectrum of interactions, PhD Thesis. Harvard University

Kim KyuHan, Choi SQ, Zasadzinski JA, Squires TM (2011) Interfacial microrheology of DPPC monolayers at the air–water interface. Soft Matter 7:7782–7789

Kim J, Peretti J, Lahlil K, Boilot J-P, Gacoin T (2013) Optically Anisotropic Thin Films by Shear-Oriented Assembly of Colloidal Nanorods. Adv Mater 25:3295–3300

Kobayashi Y, Arai N (2017) Self-Assembly and Viscosity Behavior of Janus Nanoparticles in Nanotube Flow. Langmuir 33:736–743

Kobayashi Y, Arai N, Nikoubashman A (2020) Structure and dynamics of amphiphilic Janus spheres and spherocylinders under shear. Soft Matter 16:476–486

Komura S, Hirose Y, Nonomura Y (2006) Adsorption of colloidal particles to curved interfaces. J Chem Phys 124:241104

Kumar A, Park BJ, Tu F, Lee D (2013) Amphiphilic Janus particles at fluid interfaces. Soft Matter 9(29):6604–6617

Lattuada M, Hatton TA (2011) Synthesis, properties and applications of Janus nanoparticles. Nano Today 6:286–308

Li X, Gilchrist JF (2016) Large-area nanoparticle films by continuous automated langmuir–blodgett assembly and deposition. Langmuir 32:1220–1226

Liu RC, Raman AKY, Shaik I, Aichele C, Kim SJ (2018) Inorganic microfiltration membranes incorporated with hydrophilic silica nanoparticles for oil-in-water emulsion separation. Journal of Water Process Engineering 26:124–130

Maestro A, Deshmukh OS, Mugele F, Langevin D (2015) Interfacial Assembly of Surfactant-Decorated Nanoparticles: On the Rheological Description of a Colloidal 2D Glass. Langmuir 31:6289–6297

Manga MS, Hunter TN, Cayre OJ, York DW, Reichert MD, Anna SL, Walker LM, Williams RA, Biggs SR (2016) Measurements of submicron particle adsorption and particle film elasticity at oil–water interfaces. Langmuir 32:4125–4133

Mendoza AJ, Guzmán E, Martínez-Pedrero F, Ritacco H, Rubio RG, Ortega F, Starov VM, Miller R (2014) Particle laden fluid interfaces: Dynamics and interfacial rheology. Adv Coll Interface Sci 206:303–319

Nai J, Guan BY, Le Yu, Lou XW (2017) Oriented assembly of anisotropic nanoparticles into frame-like superstructures. Sci Adv 3:e1700732

Owoseni O, Nyankson E, Zhang Y, Adams DJ, He J, Spinu L, McPherson GL, Bose A, Gupta RB, John VT (2016) Interfacial adsorption and surfactant release characteristics of magnetically functionalized halloysite nanotubes for responsive emulsions. J Colloid Interface Sci 463:288–298

Paiva FL, Hore MJA, Secchi A, Calado V, Maia J, Khani S (2020) Dynamic Interfacial Trapping of Janus Nanorod Aggregates. Langmuir 36:4184–4193

Park BJ, Lee D (2014) Particles at fluid–fluid interfaces: From single-particle behavior to hierarchical assembly of materials. MRS Bull 39:1089–1098

Park BJ, Brugarolas T, Lee D (2011) Janus particles at an oil–water interface. Soft Matter 7:6413–6417

Park B, Fuquan T, Lee DH (2013) Amphiphilic Janus particles at fluid interfaces. Soft Matter 9

Pawar AB, Kretzschmar I (2010) Fabrication, Assembly, and Application of Patchy Particles. Macromol Rapid Commun 31:150–168

Pickering SU (1907) CXCVI.—Emulsions. J Chem Soc Trans 91:2001–2021

Poh L, Narimissa E, Wagner MH, Winter HH (2022) Interactive Shear and Extensional Rheology—25 years of IRIS Software. Rheol Acta 61:259–269

Chen Q, Telmadarreie A, Dong M, Bryant S (2019) Synergistic effect between Surfactant and Nanoparticles on the stability of methane foam in EOR processes. In SPE Western Regional Meeting, 16. San Jose, California, USA: Society of Petroleum Engineers

Qiao Y, Ma X, Liu Z, Manno MA, Keim NC, Cheng X (2022) Tuning the rheology and microstructure of particle-laden fluid interfaces with Janus particles. J Colloid Interface Sci 618:241–247

Ramsden W (1904) Separation of solids in the surface-layers of solutions and 'suspensions' (observations on surface-membranes, bubbles, emulsions, and mechanical coagulation).—Preliminary account. Proc R Soc Lond 72:156–164

Razavi S, Cao KD, Lin B, Ka YC, Lee RS, Tu, and Ilona Kretzschmar. (2015) Collapse of Particle-Laden Interfaces under Compression: Buckling vs Particle Expulsion. Langmuir 31:7764–7775

Razavi S, Lin B, Ka YC, Lee RS, Tu, and Ilona Kretzschmar. (2019) Impact of Surface Amphiphilicity on the Interfacial Behavior of Janus Particle Layers under Compression. Langmuir 35:15813–15824

Razavi S, Hernandez LM, Read A, Vargas WL, Kretzschmar I (2020) Surface tension anomaly observed for chemically-modified Janus particles at the air/water interface. J Colloid Interface Sci 558:95–99

Renggli D, Alicke A, Ewoldt RH, Vermant J (2020) Operating windows for oscillatory interfacial shear rheology. J Rheol 64:141–160

Rezvantalab H, Shojaei-Zadeh S (2013) Role of Geometry and Amphiphilicity on Capillary-Induced Interactions between Anisotropic Janus Particles. Langmuir 29:14962–14970

Rezvantalab H, Connington KW, Shojaei-Zadeh S (2016) Shear-induced interfacial assembly of Janus particles. Physical Review Fluids 1:074205

Samaniuk JR, Hermans E, Verwijlen T, Pauchard V, Vermant J (2015) Soft-glassy rheology of asphaltenes at liquid interfaces. J Dispersion Sci Technol 36:1444–1451

Shah AA, Schultz B, Zhang W, Glotzer SC, Solomon MJ (2015) Actuation of shape-memory colloidal fibres of Janus ellipsoids. Nat Mater 14:117–124

Siebenbürger M, Fuchs M, Winter H, Ballauff M (2009) Viscoelasticity and shear flow of concentrated, noncrystallizing colloidal suspensions: Comparison with mode-coupling theory. J Rheol 53:707–726

Spicer PT, Gilchrist JF (2015) Microstructure, rheology, and processing of complex fluids. Adv Ind Mixing 87–114

Tein YS, Thompson BR, Majkrzak C, Maranville B, Renggli D, Vermant J, Wagner NJ (2022) Instrument for measurement of interfacial structure–property relationships with decoupled interfacial shear and dilatational flow:"Quadrotrough." Rev Sci Instrum 93:093903

Trevenen S, Hamilton HSC, Ribbe AE, Bradley LC, Beltramo PJ (2022) 'Nanoscale porosity in microellipsoids cloaks interparticle capillary attraction at fluid interfaces'. https://doi.org/10.26434/chemrxiv-2022-0g593

Tschoegl NW (2012) The phenomenological theory of linear viscoelastic behavior: an introduction. Springer Science & Business Media

Tu FQ, Lee D (2014) Shape-Changing and Amphiphilicity-Reversing Janus Particles with pH-Responsive Surfactant Properties. J Am Chem Soc 136:9999–10006

Vandebril S, Franck A, Fuller GG, Moldenaers P, Vermant J (2010) A double wall-ring geometry for interfacial shear rheometry. Rheol Acta 49:131–144

Vishal B, Ghosh P (2019) The effect of silica nanoparticles on the stability of aqueous foams. J Dispersion Sci Technol 40:206–218

Walther A, Müller AHE (2013) Janus Particles: Synthesis, Self-Assembly, Physical Properties, and Applications. Chem Rev 113:5194–5261

Weston JS, Jentoft RE, Grady BP, Resasco DE, Harwell JH (2015) Silica Nanoparticle Wettability: Characterization and Effects on the Emulsion Properties. Ind Eng Chem Res 54:4274–4284

Winter HH (1997) Analysis of dynamic mechanical data: inversion into a relaxation time spectrum and consistency check. J Non-Newt Fluid Mech 68:225–239

Winter HH (2013) Glass transition as the rheological inverse of gelation. Macromolecules 46:2425–2432

Wu H, Gao K, Yao Lu, Meng Z, Gou C, Li Z, Yang M, Ming Qu, Liu T, Hou J, Kang W (2020) Silica-based amphiphilic Janus nanofluid with improved interfacial properties for enhanced oil recovery. Colloids Surf, A 586:124162

Xue Z, Worthen A, Qajar A, Robert I, Bryant SL, Huh C, Prodanović M, Johnston KP (2016) Viscosity and stability of ultra-high internal phase CO2-in-water foams stabilized with surfactants and nanoparticles with or without polyelectrolytes. J Colloid Interface Sci 461:383–395

Zang DY, Rio E, Langevin D, Wei B, Binks BP (2010) Viscoelastic properties of silica nanoparticle monolayers at the air-water interface. The European Physical Journal E 31:125–134

Zhang J, Grzybowski BA, Granick S (2017) Janus Particle synthesis, assembly, and application. Langmuir 33:6964–6977

Zhou J, Qiao X, Binks BP, Sun K, Bai M, Li Y, Liu Y (2011) Magnetic Pickering emulsions stabilized by Fe3O4 nanoparticles. Langmuir 27:3308–3316